Optical Flow Computation Using Extended Constraints

Alberto Del Bimbo, *Member, IEEE*, Paolo Nesi, *Member, IEEE*, and Jorge L. C. Sanz, *Senior Member, IEEE*

Abstract— **Several approaches for optical flow estimation use partial differential equations to model changes in image brightness throughout time. A commonly used equation is the so-called optical flow constraint (OFC), which assumes that the image brightness is stationary with respect to time. More recently, a different constraint referred to as the extended optical flow constraint (EOFC) has been introduced, which also contains the divergence of the flow field of image brightness. There is no agreement in the literature about which of these constraints provides the best estimation of the velocity field. In this paper, two new solutions for optical flow computation are proposed, which are based on an approximation of the constraint equations. The two techniques have been used with both EOFC and OFC constraint equations. Results achieved by using these solutions have been compared with several well-known computational methods for optical flow estimation in different motion conditions. Estimation errors have also been measured and compared for different types of motion.**

I. Introduction

MOTION analysis from image sequences addresses the estimation of the relative movements between the objects in the scene and the TV camera. Interest in this research subject originates from the fields of 3-D object reconstruction [1], [2], object tracking [3]–[5], and robot navigation [6], [7].

Basically, three approaches are considered in the literature for motion estimation: matching (correspondence), spatio-temporal filtering, and the gradient-based approach. In the first approach, local matching techniques are used to evaluate the displacements in consecutive frames for selected elements (lines, corners, patterns, etc.) of the moving objects [8], [9]. Finding a sufficient number of point correspondences in consecutive frames allows direct estimation of the 3-D motion of the object under observation [10], [11]. In the second approach, the estimation of motion is obtained by filtering in both the temporal and frequency domains. Filtering is tuned in frequency and space in order to detect the motion components. Typically, these techniques do not operate over the local information but use all the information contained in the whole image sequence [12]–[14]. In the gradient-based approach, the brightness changes in the image flow are considered, thus leading to motion estimation [15]–[20]. The flow field of these changes is commonly referred to as "optical flow" or "image flow." Generally speaking, the optical flow differs from the perspective projection of the 3-D motion on the image plane (commonly referred to as "velocity field" or "motion field") [21]–[24]. Nevertheless, in many applications, the optical flow is a good approximation of the true motion in the image sequence.

Typically, optical flow estimation techniques use partial derivative constraint equations that model changes in image brightness throughout time. A commonly used constraint is the so-called optical flow constraint (OFC), which is similar to the continuity equation of fluid-dynamics and assumes that image brightness is stationary with respect to time.

Two main approaches for the computation of optical flow can be found in the literature: *regularization-* and *multiconstraint-based* approaches.

In the *regularization-based* approach, the optical flow field estimation is considered as an ill-posed problem in the sense of Hadamard [25], and solutions are obtained by minimizing a functional where a smoothness constraint is appropriately weighted to regularize the solution. Usually, methods based on this approach lead to iterative solutions, and the velocity is evaluated at every point in the image. Regularization-based approaches using the OFC have been presented in the literature [16], [17], [26]–[29]. Typically, these methods yield "dense" optical flow fields in the sense that the estimation process evaluates the optical flow field that is also inside the objects in motion and not only on the object contours. Drawbacks in the regularization-based approach are related to the fact that problems occur in the presence of object occlusions. In this case, the velocity exhibits discontinuities on the boundaries, and there is the undesirable effect that the optical flow field of one object propagates inside the overlapped objects, where the depth of propagation depends on the number of iterations and on the weighting factor. The regularization processes in many cases lead to smooth very important information about the object shape [29]. Regularization-based techniques that evaluate the optical flow only on the contours of the moving objects have been presented in [8] and [30].

The *multiconstraint-based* approach to optical flow estimation is based on the observation that the stationariness condition—assumed for the image brightness in the definition of the OFC—can also be made valid for any motion-invariant

Manuscript received May 29, 1993; revised August 5, 1995. The associate editor coordinating the review of this paper and approving it for publication was Prof. Robert M. Haralick.

A. Del Bimbo is with the Department of Systems and Informatics, University of Florence, Florence, Italy.

P. Nesi was with the Computer Science Department, IBM Almaden Research Center, San Jose, CA, USA. He is now with the Department of Systems and Informatics, University of Florence, Florence, Italy (e-mail: nesi@ingfi1.ing.unifi.it).

J. L. C. Sanz was with the Computer Research and Advanced Applications Group, IBM Argentina, Buenos Aires, Argentina. He is now with Coordinated Science Laboratory, University of Illinois at Urbana-Champaign, Urbana, IL, USA.

Publisher Item Identifier S 1057-7149(96)03165-X.

function F, where F may represent any function such as contrast, entropy, average, variance, curvature, gradient magnitude, moments of local intensity, color spectrum, images obtained with different light sources, etc. By using a set of these constraints evaluated at the same point in the image, a solvable system of equations with optical flow components as unknowns can be obtained [31], [32]. Other less generic methods adopt different constraints with second-order partial derivatives of the image brightness [18]–[20]. Multiconstraint-based solutions are solved with traditional numerical methods for the inversion or pseudoinversion of the coefficient matrix. Results obtained with these techniques strongly depend on the choice of F functions used to build the set of constraints. Other researchers have assumed that the constraints evaluated in a set of neighboring pixels on the image represent the same velocity as a first approximation, provided that the optical flow field under observation is very smooth. Therefore, a set of similar constraints in a neighborhood of a pixel yields an overdetermined system of equations for optical flow estimation. This approach is usually called *multipoint* method [33]. Multipoint solutions were proposed in [34], where an error term was added and estimated together with the optical flow field, and in [35], where a multipoint technique with a linearized version of the OFC was used in a large neighborhood of each image point.

In the multiconstraint-based approaches, different methods are used to obtain smooth solutions:

i) prefiltering to regularize the initial data (sequence of images) [34], [20], [31],
ii) a large neighborhood, collecting a large number of constraints [35],
iii) post-filtering on the estimated optical flow fields [20].

Unfortunately, these operations also result in some imprecision in the measure of the moving object boundaries since a kind of diffusion occurs.

More recently, a different constraint equation has been introduced, which also contains the divergence of the flow field of the image brightness [36]. This was obtained on the basis of the work presented in [37], as widely discussed in [24]. In the following, this equation will be referred to as extended optical flow constraint (EOFC). EOFC has been analyzed by a few authors [21], [23], [24]. As to the selection between these two constraint equations, there is no agreement in the literature about which of these two constraints provides the best estimation of the velocity field. Their analytical comparison has been carried out by the authors in [24]. To the best of our knowledge, no solutions for optical flow estimation based on EOFC have been proposed.

In this paper, two new techniques for the estimation of optical flow are discussed, which are based on an approximation of the partial differential equation modeling the changes in the image brightness. These two techniques have been used both with EOFC and OFC constraint equations. A comparison is carried out with gradient-based selected solutions previously presented in the literature under the most significant 3-D motion conditions. A comparison is also carried out with respect to the computational complexity.

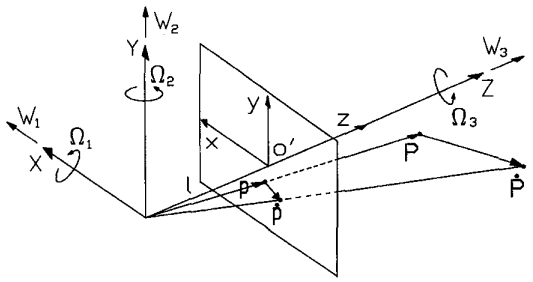

Fig. 1. Camera geometry and apparent motion.

This paper is organized as follows: Equations modeling the velocity field and the optical flow are reviewed by using a unified notation in Section II as in [24]. In Section III, the new solutions for estimating optical flow are presented. In Section IV, a comparison over a wide set of test images is carried out between the new solutions presented in this paper and selected solutions from the literature and, in many cases, estimating errors with respect to the true velocity field. Finally, conclusions are drawn in Section V.

II. Basic Notions

In this section, equations modeling the velocity field and optical flow with their constraint equations are briefly reviewed.

The Velocity Field: The velocity field is defined as the perspective projection on the image plane of the real 3-D object velocity [38]. Given a point P in the 3-D space, identified by vector[1] $\mathbf{P} = (X, Y, Z)^t$, point $\mathbf{p} = (x, y, l)^t$ is its perspective projection on the image plane at focal length $Z = l$, where x, y, l are taken with reference to the system of coordinates centered in o' (see Fig. 1). Therefore, the following relationship holds: $\mathbf{p} = \frac{l}{Z}\mathbf{P}$, and the projection of the 3-D motion on the image plane can be obtained by taking derivatives. Considering that the 3-D motion of the generic point $\mathbf{P}$ can be modeled as comprised of translational $\mathbf{W} = (W_1, W_2, W_3)^t$ and rotational $\mathbf{\Omega} = (\Omega_1, \Omega_2, \Omega_3)^t$ velocity components, two scalar equations are obtained for the two components of velocity field

$$\dot{p}_1 = \frac{lW_1}{Z} - x\frac{W_3}{Z} + l\Omega_2 - y\Omega_3 - x\frac{y\Omega_1 - x\Omega_2}{l}, \quad (1)$$

$$\dot{p}_2 = \frac{lW_2}{Z} - y\frac{W_3}{Z} + x\Omega_3 - l\Omega_1 - y\frac{y\Omega_1 - x\Omega_2}{l}. \quad (2)$$

The Optical Flow Constraint: The change in the image brightness $E(x(t), y(t), t)$ with respect to t is

$$\frac{dE}{dt} = \frac{\partial E}{\partial x}\frac{dx}{dt} + \frac{\partial E}{\partial y}\frac{dy}{dt} + \frac{\partial E}{\partial t}. \quad (3)$$

If the image brightness of each point in the image is supposed to be stationary with respect to the time variable (i.e., $dE/dt = 0$), then the following expression holds:

$$E_x u + E_y v + E_t = 0 \quad (4)$$

where the abbreviation for partial derivatives of the image brightness has been introduced, and u, v correspond to

[1] For the sake of clarity in the notation, vectors will be referred to in boldface in the following discussion.

$dx/dt, dy/dt$, representing the components of the local velocity vector $\mathbf{V}$ along the x and y directions, respectively. Equation (4) is usually called the "optical flow constraint" (OFC), and its solutions are referred to as "optical flow" or "image flow," and, in general, represent only an approximation of the velocity field $\dot{\mathbf{p}}$ [24].

The Extended Optical Flow Constraint: According to the observation that the OFC is very similar to the continuity equation of fluid dynamics, a more general motion constraint equation (relating the density of the image brightness feature derivatives and the components of the local velocity vector and its derivatives) was early presented by Schunck in [37]

$$\nabla \cdot (E\mathbf{d}) + \frac{\partial E}{\partial t} = 0 \tag{5}$$

where

$$\nabla \cdot (E\mathbf{d}) = \mathbf{d} \cdot \nabla E + E \nabla \cdot \mathbf{d} \tag{6}$$

where $\mathbf{d}$ is a different optical flow with respect to that defined with the OFC [24]. Since the image brightness is the limit, for the vanishing of the ratio between the power received by an image plane element and the size of this element [39], [40] (i.e., it is an energy density usually expressed in Watt/m^2), in [36], a conceptually new constraint equation, with the above structure, was introduced and called the extended optical flow constraint (EOFC)

$$E_x u + E_y v + E u_x + E v_y + E_t = 0 \tag{7}$$

where the same notation of OFC has been used for the optical flow field defined by this constraint equation. From the structural point of view, the EOFC equation (5) differs from the OFC equation (4) only in the term involving the divergence of the optical flow field vector ($E\nabla \cdot \mathbf{V}$). If the EOFC is supposed to be the true expression of the optical flow field, the OFC can be considered to be valid only in the region where the divergence of the optical flow field $\mathbf{V}$ is equal to zero. It is worth noting that this term vanishes only for motions that are parallel to the image plane.

III. New Techniques Based on EOFC and OFC

In this section, two new solutions for optical flow estimation based on an approximation of the EOFC equation are presented. Two additional new OFC-based solutions are also derived by using the same approach, for comparison purposes. All of them belong to the class of the multiconstraint-based approaches.

A. EOFC-Based Solutions

Let $\mathbf{p} = (x, y)$ be the perspective projection on the image plane of a point P in the 3-D space. Assume that the optical flow changes following a law that is approximately linear with $\mathbf{p}$. A linear approximation of the EOFC model around the point under consideration $\mathbf{p}_o$ can be obtained by considering that the changes of every element of the EOFC equation have at most a linear dependence on $d\mathbf{p}$ in each location $(\mathbf{p}_o + d\mathbf{p})$ at time t. Therefore, the EOFC can be rewritten as

$$E_t(\mathbf{p}_o + d\mathbf{p}, t) + \nabla E(\mathbf{p}_o + d\mathbf{p}, t) \cdot \mathbf{V}(\mathbf{p}_o + d\mathbf{p}, t) + E(\mathbf{p}_o + d\mathbf{p}, t)(u_x(\mathbf{p}_o + d\mathbf{p}, t) + v_y(\mathbf{p}_o + d\mathbf{p}, t)) = 0. \tag{8}$$

By using the first-order approximation of every term and considering the components up to the second order in dx, dy, (8) can be written as

$$\begin{aligned}&(E_t + E_x u + E_y v + E u_x + E v_y)\\ &\quad + (E_{tx} + E_{xx} u + E_{yx} v + 2E_x u_x + E_y v_x\\ &\qquad + E_x v_y + E u_{xx} + E v_{yx}) dx\\ &\quad + (E_{ty} + E_{xy} u + E_{yy} v + E_y u_x + E_x u_y\\ &\qquad + 2E_y v_y + E u_{xy} + E v_{yy}) dy = 0.\end{aligned} \tag{9}$$

Numerical solutions are obtained in the discrete domain since images are sampled on a fixed grid of points at regular time intervals. In the following, an image will be considered to be the discrete collection of the irradiance measures $E_{i,j,t}$ for $i = 1, \cdots, M$ and $j = 1, \cdots, M$ along the x and y axes, respectively.

If the optical flow follows a law that is approximately linear in (x, y), a smoothed solution for optical flow estimation can be obtained by using a linear approximation of the constraint in the $N \times N$ neighborhood of each point on the grid. This assumption is valid only if the optical flow field under observation is smooth.

First-Order EOFC-Based Solution: A first-order solution is obtained, assuming that (9) vanishes for all the $d\mathbf{p}$ components. This condition will be satisfied if the following systems are verified:

$$E_t + E_x u + E_y v + E u_x + E v_y = 0 \tag{10a}$$

$$E_{tx} + E_{xx} u + E_{yx} v + 2E_x u_x + E_y v_x + E_x v_y + E u_{xx} + E v_{yx} = 0 \tag{10b}$$

$$E_{ty} + E_{xy} u + E_{yy} v + E_y u_x + E_x u_y + 2E_y v_y + E u_{xy} + E v_{yy} = 0. \tag{10c}$$

Neglecting the second-order derivatives of the velocity field $(u_{xx}, v_{yx}, u_{xy}, v_{yy})$, the following system of equations for each pixel is obtained:

$$E_t + E_x u + E_y v + E u_x + E v_y = 0 \tag{11a}$$

$$E_{tx} + E_{xx} u + E_{yx} v + 2E_x u_x + E_y v_x + E_x v_y = 0 \tag{11b}$$

$$E_{ty} + E_{xy} u + E_{yy} v + E_y u_x + E_x u_y + 2E_y v_y = 0. \tag{11c}$$

These equations are used to build an overdetermined system of three $(N \times N)$ equations in six unknowns $(u, v, u_x, v_y, u_y, v_x)$. This system is formed by taking the following equations for all (i, j) in the $N \times N$ neighborhood of $\mathbf{p}_o$

$$E_{t(i,j,t)} + E_{x(i,j,t)} u + E_{y(i,j,t)} v + E_{(i,j,t)} u_x + E_{(i,j,t)} v_y = 0 \tag{12a}$$

$$E_{tx(i,j,t)} + E_{xx(i,j,t)} u + E_{yx(i,j,t)} v + 2E_{x(i,j,t)} u_x + E_{y(i,j,t)} v_x + E_{x(i,j,t)} v_y = 0 \tag{12b}$$

$$E_{ty(i,j,t)} + E_{xy(i,j,t)} u + E_{yy(i,j,t)} v + E_{y(i,j,t)} u_x + E_{x(i,j,t)} u_y + 2E_{y(i,j,t)} v_y = 0 \tag{12c}$$

TABLE I
ERROR COMPARISON OF THE ESTIMATED OPTICAL FLOW FIELDS FOR THE TRANSLATIONAL MOTION. TEST SEQUENCE WITH A SUPERIMPOSED PLAID PATTERN ON THE WHOLE IMAGE. THE PATTERN WAS MOVING AT 45° WITH VELOCITY COMPONENTS (1, 1) PIXEL PER FRAME

	$N=3$				$N=5$			
algorithm	$Err_{\|\mathbf{V}\|}$	$Var_{Err_{\|\mathbf{V}\|}}$	Err_{φ}	$Var_{Err_{\varphi}}$	$Err_{\|\mathbf{V}\|}$	$Var_{Err_{\|\mathbf{V}\|}}$	Err_{φ}	$Var_{Err_{\varphi}}$
Zero-order EOFC-based	6.683	0.0013	0.037	0.0021	6.018	0.0001	0.004	0.0001
First-order EOFC-based	10.846	0.0039	0.086	0.0032	7.265	0.0003	0.018	0.0002
Zero-order OFC-based	5.695	0.0005	0.008	0.0008	5.680	0.0000	0.001	0.0001
First-order OFC-based	5.653	0.0001	0.010	0.0002	5.696	0.0000	0.008	0.0000

	$N=7$				$N=9$			
algorithm	$Err_{\|\mathbf{V}\|}$	$Var_{Err_{\|\mathbf{V}\|}}$	Err_{φ}	$Var_{Err_{\varphi}}$	$Err_{\|\mathbf{V}\|}$	$Var_{Err_{\|\mathbf{V}\|}}$	Err_{φ}	$Var_{Err_{\varphi}}$
Zero-order EOFC-based	5.732	0.0000	0.000	0.0000	5.651	0.0000	0.000	0.0000
First-order EOFC-based	6.211	0.0000	0.000	0.0000	5.835	0.0000	0.000	0.0000
Zero-order OFC-based	5.631	0.0000	0.000	0.0000	5.621	0.0000	0.000	0.0000
First-order OFC-based	5.662	0.0000	0.002	0.0000	5.652	0.0000	0.001	0.0000

	without filtering				*with Gaussian post-filtering*, $N=3$			
algorithm	$Err_{\|\mathbf{V}\|}$	$Var_{Err_{\|\mathbf{V}\|}}$	Err_{φ}	$Var_{Err_{\varphi}}$	$Err_{\|\mathbf{V}\|}$	$Var_{Err_{\|\mathbf{V}\|}}$	Err_{φ}	$Var_{Err_{\varphi}}$
Horn & Schunck, 12 It.	15.902	0.0044	0.967	0.0391	16.474	0.0023	0.986	0.0268
Horn & Schunck, 24 It.	6.271	0.0006	0.422	0.0032	6.611	0.0005	0.423	0.0022
Horn & Schunck, 36 It.	3.032	0.0001	0.163	0.0004	3.251	0.0002	0.267	0.0002
Horn & Schunck, 99 It.	1.463	0.0000	0.042	0.0000	1.804	0.0002	0.040	0.0000
Haralick & Lee	10.632	0.0035	0.167	0.0195	8.465	0.0032	0.012	0.0004
Tretiak & Pastor	7.097	0.0183	0.462	0.0385	3.464	0.0035	0.030	0.0048

	with Gaussian post-filtering, $N=5$				*with Gaussian post-filtering*, $N=7$			
algorithm	$Err_{\|\mathbf{V}\|}$	$Var_{Err_{\|\mathbf{V}\|}}$	Err_{φ}	$Var_{Err_{\varphi}}$	$Err_{\|\mathbf{V}\|}$	$Var_{Err_{\|\mathbf{V}\|}}$	Err_{φ}	$Var_{Err_{\varphi}}$
Haralick & Lee	7.61	0.0029	0.011	0.0002	7.49	0.0005	0.009	0.0002
Tretiak & Pastor	3.55	0.0034	0.034	0.0030	3.81	0.0012	0.062	0.0028

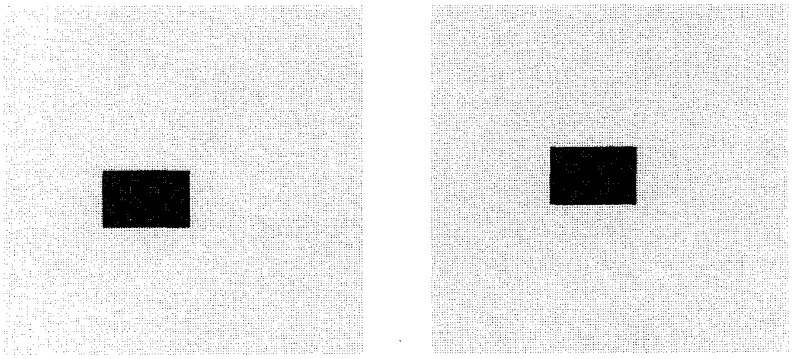

Fig. 2. Sequence of images where an object with a superimposed plaid pattern is moving at 45° with respect to the X axis (first and ninth frame, 128 × 128 image resolution).

and solving for $(u, v, u_x, v_y, u_y, v_x)$. The overdetermined system is solved by using the least-squares technique and LU decomposition.

Zeroth-Order EOFC-Based Solution: Another multipoint solution based on the EOFC could be obtained by considering only the zeroth-order components of (9), thus yielding

$$E_t + E_x u + E_y v + E u_x + E v_y = 0.$$

For the estimation of the velocity components at $\mathbf{p}_o$, an overdetermined system of $N \times N$ EOFC equations in four unknowns (u, v, u_x, v_y) can be built. Since, in the EOFC equation, the unknowns u_x, and v_y are linearly dependent on each other (having the same coefficient E), the constraint equation

$$E_{t(i,j,t)} + E_{x(i,j,t)} u + E_{y_{(i,j,t)}} v + E_{(i,j,t)} \nabla \cdot \mathbf{V} = 0 \quad (13)$$

is used to build an overdetermined linear system of $N \times N$ equations in three unknowns $(u, v, \nabla \cdot \mathbf{V})$ for all (i, j) in the $N \times N$ neighborhood of $\mathbf{p}_o$. This system is solved by using a least-squares technique.

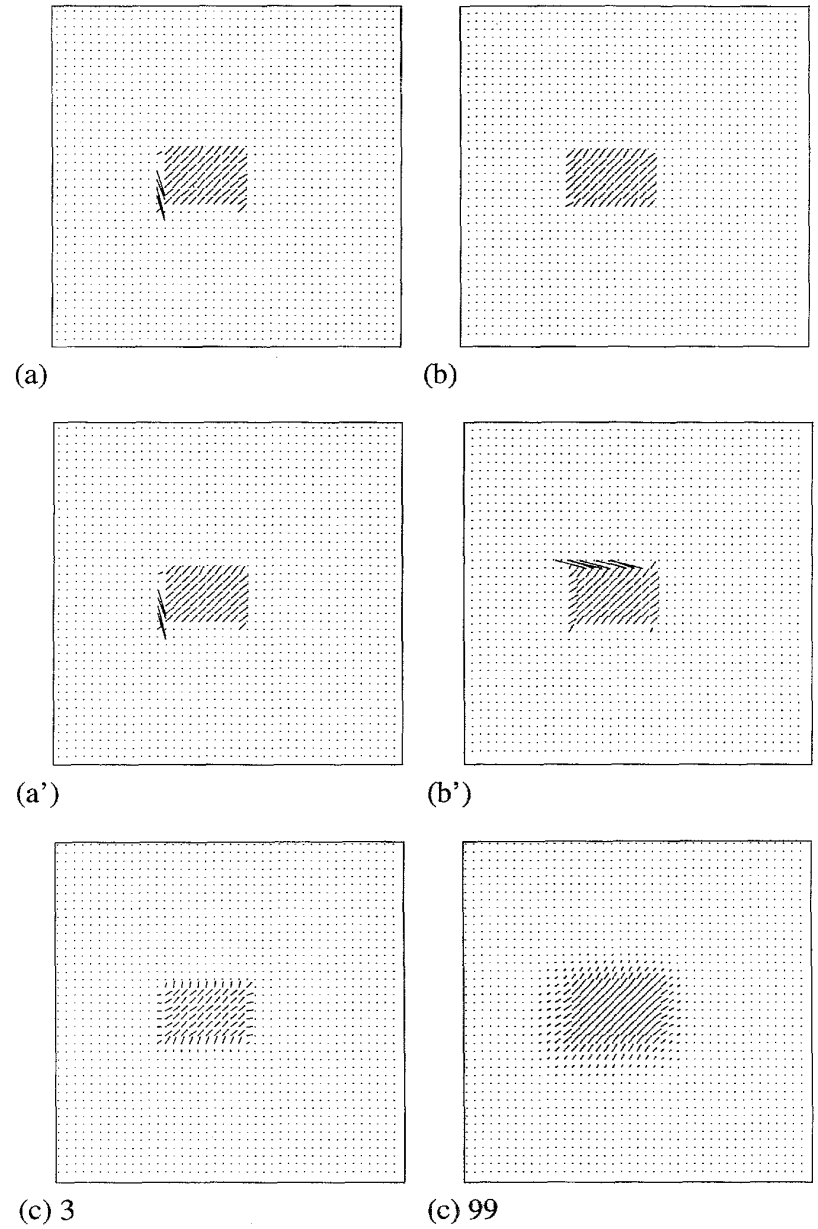

Fig. 3. Optical flow estimation referred to the fifth frame of the sequence in Fig. 2 obtained with (a) zeroth-order EOFC-based solution, $N = 3$; (b) first-order EOFC-based solution, $N = 3$; (a′) zeroth-order OFC-based solution, $N = 3$; (b′) first-order OFC-based solution, $N = 3$; (c) Horn and Schunck OFC-based solution (iterations: 3, 99), $\alpha = 0.6$; (d) Haralick and Lee multiconstraint OFC-based solution, 3×3 post-filtering; (e) Tretiak and Pastor OFC-based direct solution, 3×3 post-filtering.

B. OFC-Based Solutions

The OFC-based solutions have been obtained by following the same approach adopted for the EOFC-based solutions. In this case, the constraint (9) takes the form

$$(E_t + E_x u + E_y v) + (E_{tx} + E_{xx} u + E_{yx} v + E_x u_x + E_y v_x) dx + (E_{ty} + E_{xy} u + E_{yy} v + E_x u_y + E_y v_y) dy = 0. \quad (14)$$

First-Order OFC-Based Solution: The first-order OFC-based solution is obtained by assuming that (14) vanishes for all the $d\mathbf{p}$ components. If this condition is satisfied, three constraint equations for each pixel will be defined

$$E_t + E_x u + E_y v = 0 \quad (15a)$$

$$E_{tx} + E_{xx} u + E_{yx} v = 0 \quad (15b)$$

$$E_{ty} + E_{xy} u + E_{yy} v = 0 \quad (15c)$$

where the first-order derivatives of the optical flow field (u_x, u_y, v_x, v_y) have been neglected. These equations are used to define a multipoint solution of three $(N \times N)$ equations on two unknowns.

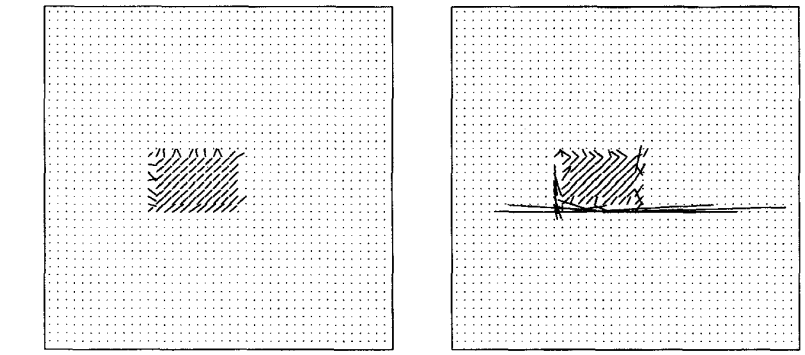

(d) (e)

Fig. 3. (Continued).

TABLE II
MEASURES OF THE ESTIMATION ERRORS FOR A MOVING PLAID PATTERN WITH THE ADDITION OF A 20% GAUSSIAN NOISE. THE PATTERN MOVES AT 45° WITH VELOCITY COMPONENTS $(1, 1)$ PIXEL PER FRAME. THE ESTIMATIONS HAVE BEEN OBTAINED IN EACH IMAGE POINT AND ASSUMING $N = 5$ FOR THE MULTIPOINT ALGORITHMS. THE GAUSSIAN FILTERING OF THE IMAGES (PREFILTERING) OR THE POSTFILTERING ON THE OPTICAL FLOW FIELDS HAVE BEEN PERFORMED BY USING A 5×5 OPERATOR WITH $\sigma = 1$

	without filtering				*with Gaussian pre-filtering*			
algorithm	$Err_{\|\mathbf{V}\|}$	$Var_{Err_{\|\mathbf{V}\|}}$	Err_{φ}	$Var_{Err_{\varphi}}$	$Err'_{\|\mathbf{V}\|}$	$Var_{Err'_{\|\mathbf{V}\|}}$	Err'_{φ}	$Var_{Err'_{\varphi}}$
Zero-order EOFC-based	33.13	0.037	2.03	0.121	8.92	0.023	0.96	0.033
First-order EOFC-based	63.43	0.024	14.32	0.449	13.80	0.020	0.66	0.027
Zero-order OFC-based	20.73	0.012	0.23	0.075	7.24	0.010	0.09	0.018
First-order OFC-based	22.10	0.012	0.34	0.053	7.87	0.009	0.27	0.014
Horn & Schunck, 12 It.	19.81	0.053	7.97	0.391	16.56	0.019	0.46	0.086
Horn & Schunck, 24 It.	15.73	0.054	6.25	0.314	7.82	0.018	0.11	0.043
Horn & Schunck, 36 It.	14.86	0.054	6.11	0.304	5.02	0.018	0.09	0.038
Horn & Schunck, 99 It.	14.61	0.054	5.94	0.054	3.74	0.018	0.10	0.036
Haralick & Lee	87.43	0.217	25.0	0.660	36.68	0.038	3.78	0.137
Tretiak & Pastor	82.20	10.82	44.0	0.960	31.05	2.455	18.06	0.457

	with Gaussian post-filtering			
algorithm	$Err''_{\|\mathbf{V}\|}$	$Var_{Err''_{\|\mathbf{V}\|}}$	Err''_{φ}	$Var_{Err''_{\varphi}}$
Haralick & Lee	16.07	0.014	1.53	0.134
Tretiak & Pastor	15.79	0.501	31.06	0.771

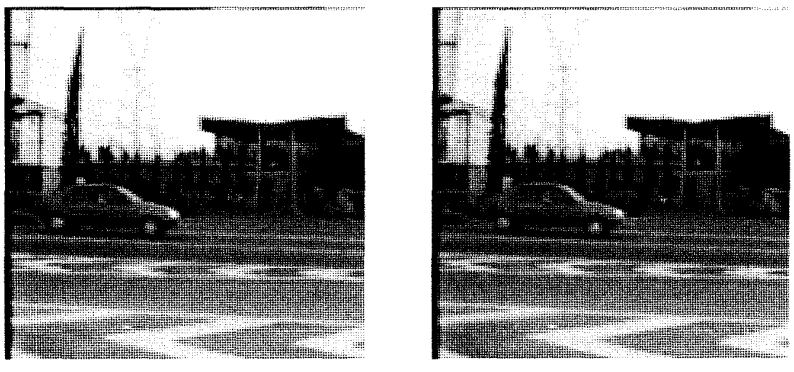

1 5

Fig. 4. Outdoor scene where a car moves in translational motion along the X-axis (first and fifth frame, 128×128image resolution).

This solution is similar to the second solution presented by Tretiak and Pastor in [19]. However, in the present approach, the three constraint equations are used in the neighborhood $(N \times N)$ of each pixel, thus defining a multipoint solution, whereas in [19], a system of three equations in two unknowns is solved for every pixel.

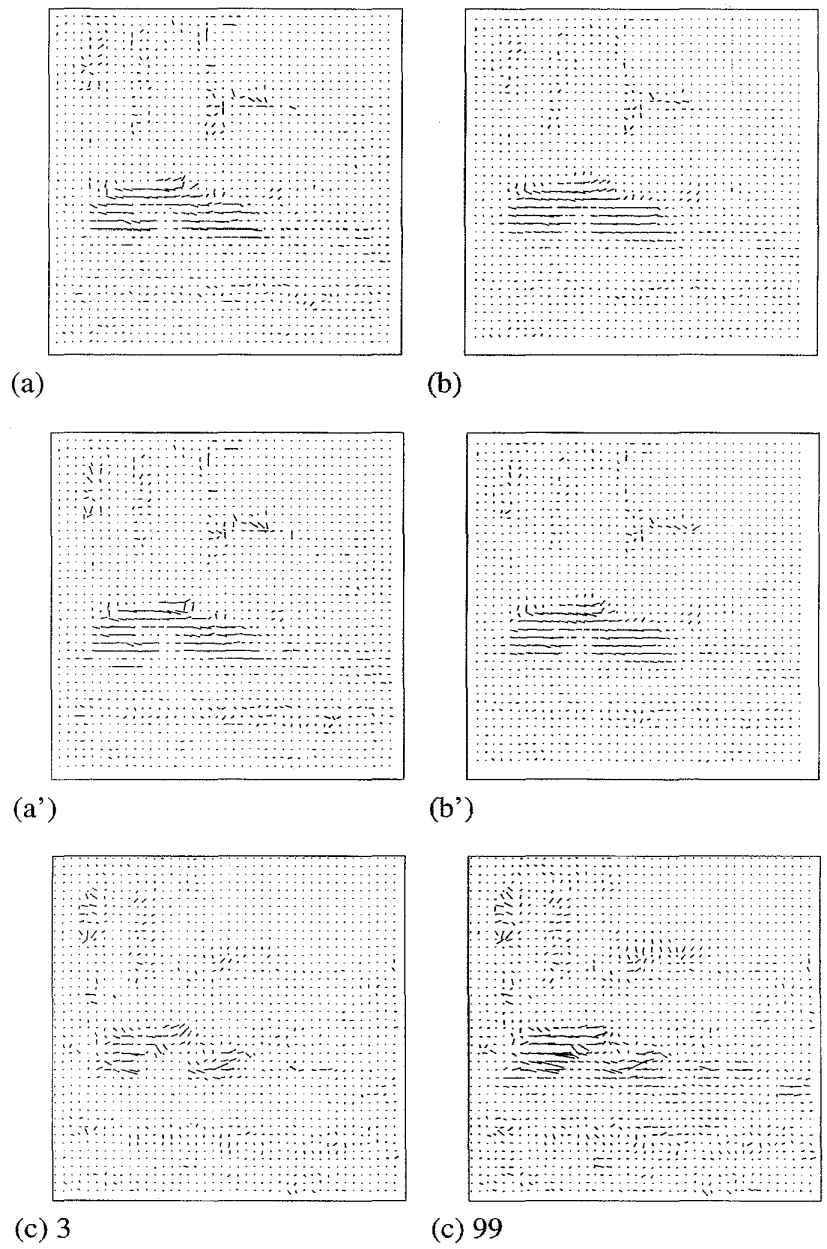

Fig. 5. Optical flow estimation referred to the third frame of the sequence in Fig. 4 obtained with (a) zeroth-order EOFC-based solution, $N = 3$; (b) first-order EOFC-based solution, $N = 3$; (a′) zeroth-order OFC-based solution, $N = 3$; (b′) first-order OFC-based solution, $N = 3$; (c) Horn and Schunck OFC-based solution (iterations: 3, 99), $\alpha = 0.6$; (d) Haralick and Lee multiconstraint OFC-based solution, 3×3 post-filtering; (e) Tretiak and Pastor OFC-based direct solution, 3×3 post-filtering.

Zeroth-Order OFC-Based Solution: The zeroth-order OFC-based solution is obtained by considering only the zeroth-order components of (14)

$$E_t + E_x u + E_y v = 0.$$

For estimating the optical flow at $\mathbf{p}_o$, an overdetermined system of $N \times N$ equations in two unknowns is defined in the $N \times N$ neighborhood. This solution is similar to that presented by Campani and Verri [35], as discussed in the Introduction.

In all the above techniques (both EOFC- and OFC-based), a large N will smooth the optical flow estimations and lead to a resolution loss.

IV. Experimental Comparisons

In this section, a comparison of the new EOFC- and OFC-based solutions with selected OFC-based approaches from the literature is carried out for different types of 3-D motion. The aperture problem [41]–[43] is not taken into account in this comparison.

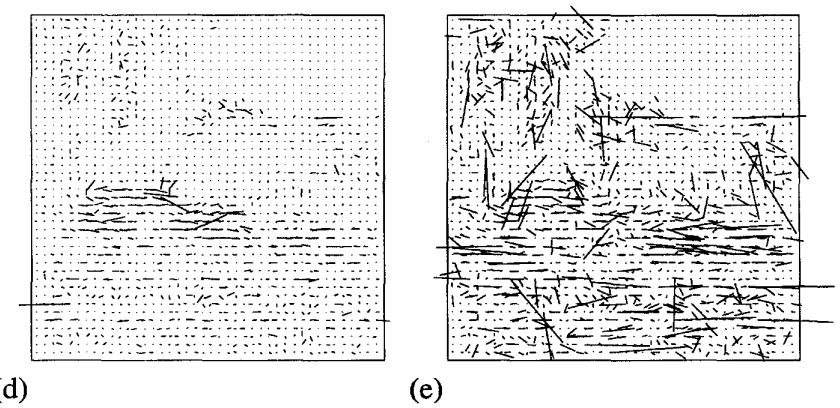

Fig. 5. (Continued).

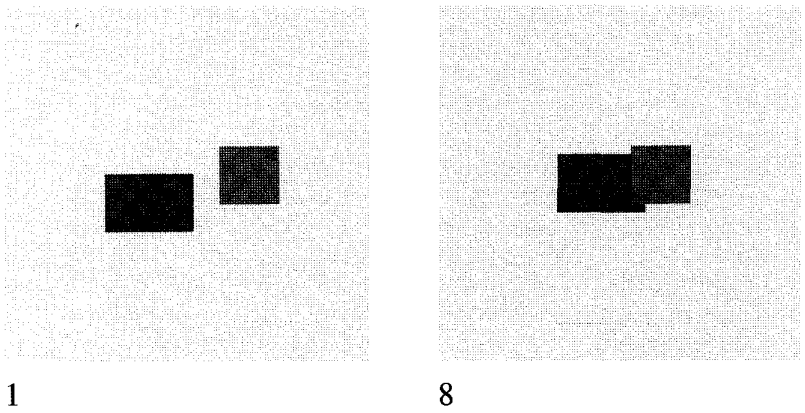

Fig. 6. Sequence of images where two objects with a superimposed plaid pattern move in opposite directions (180 and 45° with respect to the X-axis, respectively); first and eighth frame, 128 × 128 image resolution.

In particular, the solutions proposed by Horn and Schunck [16], Haralick and Lee [18], and the first solution by Tretiak and Pastor [19] have been selected for the comparison.

The solution of Horn and Schunck [16] is taken to represent the regularization-based techniques. The solution proposed by Haralick and Lee [18] is assumed to represent the class of multiconstraint-based approaches in which an overdetermined system with second-order partial derivatives of the image brightness is used, and solutions are obtained by using the pseudoinverse technique in every point in the image. This class also includes the second solution presented by Tretiak and Pastor in [19]. The first solution by Tretiak and Pastor [19] was taken as an instance of the multiconstraint approaches based on second-order partial derivatives of the image brightness, where the optical flow estimation is obtained by using a direct solution (e.g., Verri *et al.* [20], Danielsson *et al.* [44].

The new EOFC- and OFC-based solutions presented in this paper estimate the optical flow in each pixel by using the information coming from an $N \times N$ neighborhood. The algorithm of Horn and Schunck obtains the solution iteratively, and thus, the optical flow produced is due to a large neighborhood, which in turn depends on the number of iterations (i.e., at each iteration, a sort of 3×3 filtering is performed; see [16] and [29]). The solutions of Haralick and Lee, and that of Tretiak and Pastor, evaluate optical flow directly for each pixel of the whole image. Therefore, solutions are evaluated only in those points in which the system of equations are solvable. These differences in behavior make the comparison difficult; therefore, as a first step, a study for identifying comparable operating conditions has been performed.

The behavior of the algorithms for optical flow estimation is analyzed by using sequences of both synthetic and real scenes. In synthetic sequences, objects with a superimposed pattern are adopted; in these cases, isotropic illumination and calibrated systems have been provided. Sequences of real environments include both indoor (in these cases, isotropic illumination and noncalibrated optical systems have been used) and outdoor scenes (in these cases, uniform illuminations and noncalibrated optical system have been considered). For each test sequence, the optical flow fields are reported for the techniques being compared; although the optical flow fields are estimated in each image pixel, a clearer presentation is obtained when presenting the velocity vectors obtained by subsampling the fields with a grid of 3×3. A measure of the estimation errors is performed when their computation is possible, i.e., when the true velocity field is known.

In the experiments, in order to highlight the robustness of each technique, solutions are obtained with no specific method to improve optical flow quality and precision, such as the thresholding of the optical flow field magnitude for removing vectors due to discontinuities.

For the estimation of the image brightness partial derivatives, the following operators derived from that of Prewitt have been used, i.e.

$$\begin{aligned}
E_{x(i,j,t)} &= (E_{(i+1,j-1,t)} - E_{(i-1,j-1,t)} + E_{(i+1,j,t)} \\
&\quad - E_{(i-1,j,t)} + E_{(i+1,j+1,t)} - E_{(i-1,j+1,t)})/6, \\
E_{y(i,j,t)} &= (E_{(i-1,j+1,t)} - E_{(i-1,j-1,t)} + E_{(i,j+1,t)} \\
&\quad - E_{(i,j-1,t)} + E_{(i+1,j+1,t)} - E_{(i+1,j-1,t)})/6, \\
E_{t(i,j,t)} &= (E_{(i+1,j,t+1)} - E_{(i+1,j,t-1)} + E_{(i-1,j,t+1)} \\
&\quad - E_{(i-1,j,t-1)} + E_{(i,j,t+1)} - E_{(i,j,t-1)} \\
&\quad + E_{(i,j+1,t+1)} - E_{(i,j+1,t-1)} + E_{(i,j-1,t+1)} \\
&\quad - E_{(i,j-1,t-1)})/10.
\end{aligned}$$

The results obtained by using these operators have been compared with respect to other techniques (e.g., splines, B-splines, and classical interpolations) on several image sequences with known image pattern and, thus, the correct values of partial derivatives. As a result, the operators adopted present a good compromise between performance and precision and include a smoothing action since the derivatives are evaluated as the average of at least three central differences. Moreover, since the experiments have been drawn with the intention of comparison, it was observed that the adoption of more sophisticated methods for partial derivative estimation does not change sensibly either i) the relationships among the technique behavior or ii) the trends with respect to the main parameters of the techniques being compared.

A. Translational Motion

As a first experiment, the response of the algorithms under consideration with respect to the neighborhood dimension has been analyzed. To this end, a test image sequence has been defined, where a plaid pattern was superimposed on the whole image.[2] The plaid pattern has often been used in the literature for testing algorithms for optical flow estimation; it has been obtained through the combination of two sinusoidal patterns with orthogonal directions. Thus, the image brightness of the moving pattern is

$$E_{\text{obj}}(x', y') = E_b + A \sin\left(\frac{\pi x'}{2T}\right) \sin\left(\frac{\pi y'}{2T}\right)$$

where

E_b	brightness of the background,
A	amplitude of the plaid pattern,
T	period in pixel,
x', y'	relative coordinates.

[2]This has been done in order to avoid the effects of the presence of discontinuities and propagation in the computation of errors.

The pattern was moving at 45° with velocity components (1, 1) pixel per frame (i.e., translational motion).

The algorithms under comparison have been applied to the above-described image sequence in order to obtain the corresponding optical flow fields. In Table I, the measured percentage average errors of the optical flow modules ($\text{Err}_{\|\mathbf{V}\|}$) and of the direction of motion (Err_{φ}) with respect to the true velocity field are reported with their respective variances. In the first two tables, the behavior of the multipoint solutions with respect to the dimension of the neighborhood is reported for N equal to 3, 5, 7, and 9. From these tables, it can be observed that by increasing the neighborhood size, the errors decrease. In general, the errors tend to reach a limit close to the value estimated by using the zeroth-order OFC-based solution with a small value of N. On the contrary, increasing N leads to a loss in resolution. It should be noted that no strong differences exist in the results for $N = 9$, whether the OFC or the EOFC is employed. These results substantially agree with the considerations reported in [24], where it is affirmed that for translational motion, OFC and EOFC are affected by the same error in the estimation of the velocity field.

The third part of Table I reports the results obtained by applying the multiconstraint- and regularization-based algorithms in two distinct conditions: a) simple estimations without any filtering (i.e., prefiltering of the images and/or postfiltering of the optical flow) and b) estimation with postfiltering of the velocity field with a Gaussian filter of 5×5 and $\sigma = 1$.

Considering the results obtained without postfiltering, the Horn and Schunck solution presents the lowest error after a considerable number of iterations, even with respect to the multipoint solutions. This is also made easier since the velocity field under estimation is uniform, and the regularization-based algorithms tend to obtain a uniform result with the increase in the iteration number. On the contrary, the multiconstraint-based solutions present high error values. If these solutions are passed through a postfiltering with $N = 3$, an error decrease is observed. In this case, the solution of Tretiak and Pastor has a low error for the velocity module but presents a high value for the corresponding variance with respect to the other techniques. In these conditions, the solution obtained with the Horn and Schunck methods present a decrease in the variances at the expense of the module error.

In the third and fourth parts of Table I, the behavior of the multiconstraint-based algorithms with respect to the increase in the neighborhood size is reported. A wider neighborhood leads to increase the error ($\text{Err}_{\|\mathbf{V}\|}$) for the solutions of Horn and Schunck and that of Tretiak and Pastor. As can be noted, $N = 3$ can be a good compromise between precision and computational complexity. In general, postfiltering increases the precision of the vector field orientation.

For the multipoint-based solutions, the effects of the postfiltering have not been studied since these approaches present a sort of filtering for the fact that the solutions are obtained on the basis of the constraint equations coming from the neighboring pixels. It should be noted that since the images are synthetic without noise, the prefiltering technique does not improve the estimation precision.

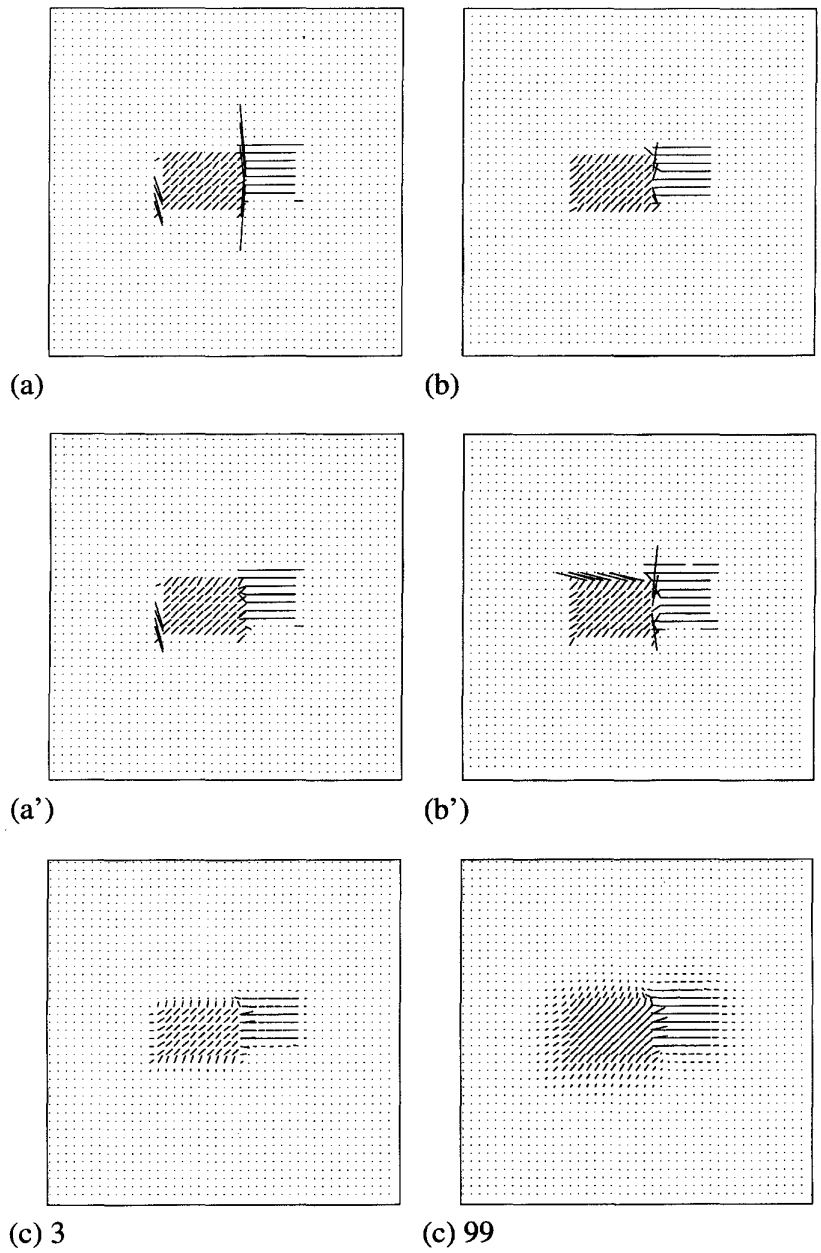

Fig. 7. Optical flow estimation referred to the fifth frame of the sequence in Fig. 6 obtained with (a) zeroth-order EOFC-based solution, $N = 3$; (b) first-order EOFC-based solution, $N = 3$; (a′) zeroth-order OFC-based solution, $N = 3$; (b′) first-order OFC-based solution, $N = 3$; (c) Horn and Schunck OFC-based solution (iterations: 3, 99), $\alpha = 0.6$; (d) Haralick and Lee multiconstraint OFC-based solution, 3×3 post-filtering; (e) Tretiak and Pastor OFC-based direct solution, 3×3 post-filtering.

In general, by observing the above-mentioned tables, it can be noted that a comparison between the multipoint solutions and the other solutions can be performed by considering the multipoint solutions that have a neighborhood dimension equal to the dimension of Gaussian postfiltering adopted in the multiconstraint-based solutions. In this way, a comparable computational effort is chosen, and the estimations are produced, considering the information coming at least from the same neighboring pixels. For these reasons, in most of the following experiments, the algorithms are compared by considering $N \times N$ neighboring pixels for the multipoint solutions and an $N \times N$ postfiltering for the others. Moreover, since the Horn and Schunck algorithm presents a smoothing at each iteration on the 3×3 neighborhood, $N = 3$ has often been used in the rest of the experiments.

B. Discontinuities in Optical Flow

The structure of the constraint equations and the presence of discontinuities make the problem of optical flow estimation ill posed [25]. Discontinuities arise from the presence of noise,

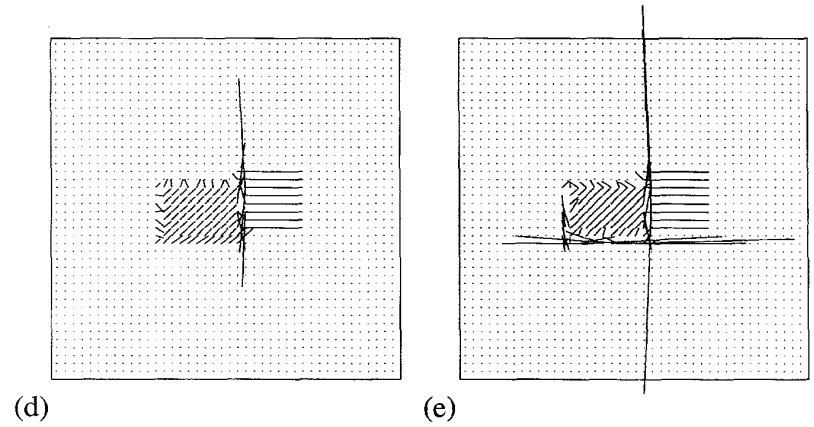

Fig. 7. (Continued).

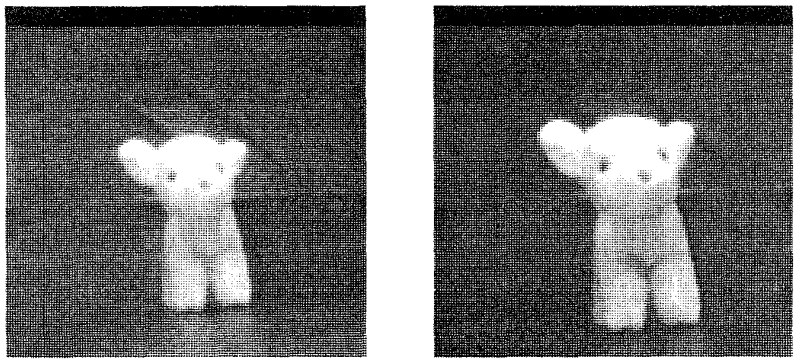

Fig. 8. Sequence of images obtained by moving the camera toward the scene along the Z axis (first and 15th frame, 128×128 image resolution).

TABLE III
ROTATIONAL VELOCITIES AND ERRORS ESTIMATED FOR THE SEQUENCE IN FIG. 12. THE PATTERN WAS ROTATING AT 4.625° PER FRAME

algorithm	$\|\Omega_3\|$	$Err_{\|\Omega_3\|}$
Zero-order EOFC-based	4.600	0.53
First-order EOFC-based	4.711	1.87
Zero-order OFC-based	4.609	0.33
First-order OFC-based	4.487	2.97
Horn & Schunck, 24th Iteration	3.910	15.44
Horn & Schunck, 42th Iteration	4.861	5.10
Horn & Schunck, 99th Iteration	4.864	5.18
Haralick & Lee	4.347	5.99
Tretiak & Pastor	4.914	6.25

patterns on the moving object surfaces that are too crisp, occlusions between moving objects or among the moving objects and the background, and object velocities with respect to the measurement system that are too fast. These difficulties can be overcome (or simply attenuated) by convolving the image with a 2-D or 3-D Gaussian smoothing operator. However, crisp patterns are also a useful feature to evaluate the optical flow.

As a general consideration, the approaches based on second-order derivatives of the image brightness (especially derivatives with respect to time t) are very sensitive to discontinuities [18], [19]. The new solutions presented in this paper use an overdetermined system of equations to reduce the effects of discontinuities so that postfiltering is not needed. The smoothness of the solution can be improved by augmenting the size of the $N \times N$ neighborhood area, even at the expense of loss of resolution of object boundaries. Results presented in the following for different types of discontinuities have been obtained with $N = 3$ by using a postfiltering for the multiconstraint-based solutions. The new algorithms are less sensitive to the discontinuities than those used for comparison with the same neighborhood dimension N.

Object Boundaries: The sequence in Fig. 2, where a rectangle is moving with translational motion at 45° with respect to the X axis, is used to test the different solutions for translational motion and moving object boundaries. A plaid pattern was superimposed to the object.

In Fig. 3, the results obtained with the techniques under analysis are shown by considering $N = 3$ for the multipoint solution and a postfiltering of the optical flow estimated with a Gaussian filter on a 3×3 area with $\sigma = 1$ for the multiconstraint-based solutions. In all the solutions considered, due to the presence of the pattern on the moving object, the

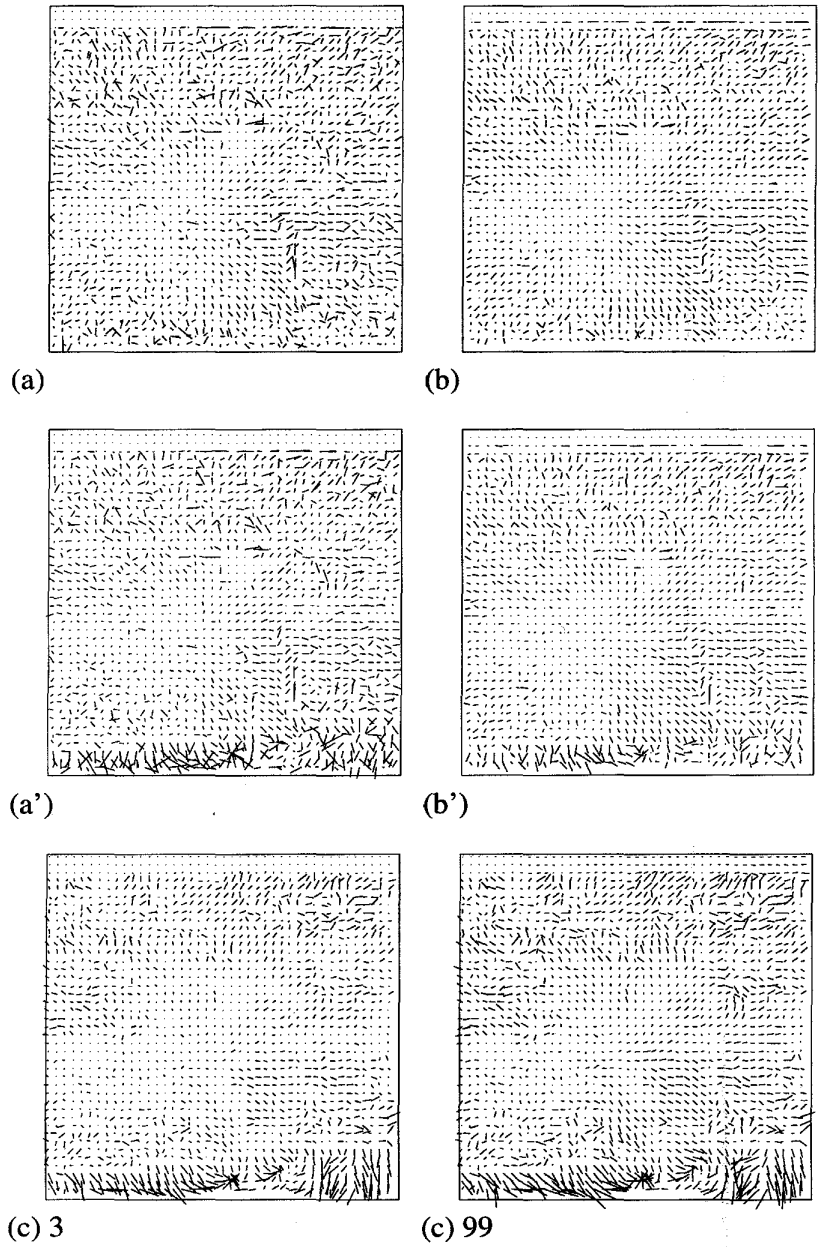

Fig. 9. Optical flow estimation referred to the fifth frame of the sequence in Fig. 8 obtained with (a) zeroth-order EOFC-based solution, $N = 3$; (b) first-order EOFC-based solution, $N = 3$; (a′) zeroth-order OFC-based solution, $N = 3$; (b′) first-order OFC-based solution, $N = 3$; (c) Horn and Schunck OFC-based solution (iterations: 3, 99), $\alpha = 0.6$; (d) Haralick and Lee multiconstraint OFC-based solution, 3×3 post-filtering; (e) Tretiak and Pastor OFC-based direct solution, 3×3 post-filtering.

optical flow field is also estimated inside the object boundaries. Fig. 3 shows that no appreciable difference exists among the solutions inside the moving objects. It should be noted that the approach by Horn and Schunck provides more satisfactory results with respect to the zeroth-order EOFC-based solution only after 40 iterations.

Fig. 3 shows that the solution of Tretiak and Pastor presents a higher sensitivity to the discontinuities on the boundaries with respect to the other solutions. For the Horn and Schunck solution, it should be observed that the velocity vectors obtained at the early iterations along the object boundaries are parallel to ∇E (see Fig. 3). On the other hand, observing the result at the 99th iteration, it can be noted that the iterative process has regularized the direction of flow at the expense of the object shape resolution. First-order EOFC- and OFC-based solutions provide better results than the corresponding zeroth-order solutions due to the higher number of constraint equations per pixel that have been used.

Noise: Sensitivity to noise was tested by using two image sequences: i) a sequence of frames in an outdoor environment,

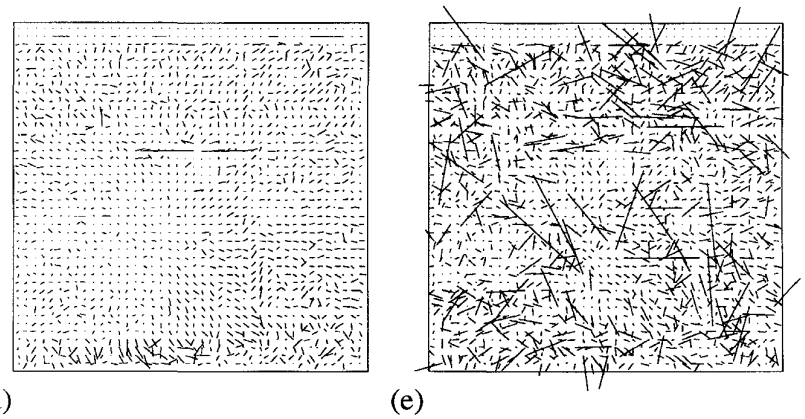

(d) (e)

Fig. 9. (Continued).

where a car is moving by translational motion (see Fig. 4); and ii) the same image sequence of the first test (e.g., a moving plaid pattern covering the whole image) but with the addition of a 20% of Gaussian noise. Results for sequence i) are reported in Fig. 5. A lower sensitivity to noise for the first-order EOFC- and OFC-based solutions with respect to the zeroth-order solutions can be observed in Fig. 5. This is due to the higher number of constraints used in the first-order solutions, which also lead to smoother solutions. It can also be noted by observing the error variances obtained for sequence ii) in Table II. This also results in a greater robustness from the computational point of view.

The approach of Tretiak and Pastor is the most sensitive to noise (see Fig. 5(e)). In this approach, a final averaging (a particular kind of postfiltering) with a large window (for example, 30×30) could be performed, leading to a significant improvement in quality. However, this produces imprecision in the measurement of the moving object boundaries. In the regularization-based technique (see Fig. 5(c)), noise effects are reduced in the early iteration steps. On the other hand, as the number of iterations becomes large, the spurious velocity vectors due to noise are enhanced (see Fig. 5(c)), thus leading to incorrect velocity vectors.

In Table II, the estimation error values are reported for noise analysis on the image sequence ii). Error percentages are derived by considering estimations without any filtering action for all the estimation techniques $(\mathrm{Err}_{\|\mathbf{V}\|}, \mathrm{Err}_{\varphi})$, estimations after having applied a 2-D Gaussian filtering $5 \times 5(\sigma = 1)$ to the sequence frames (i.e., prefiltering) $(\mathrm{Err}'_{\|\mathbf{V}\|}, \mathrm{Err}'_{\varphi})$, and estimations after a postfiltering $(5 \times 5, \sigma = 1, \mathrm{Err}''_{\|\mathbf{V}\|}, \mathrm{Err}''_{\varphi})$ of estimated optical flow fields. It should be observed that different noise sensitivities are obtained for the cases.

The solution by Horn and Schunck provides the best result but with a very large number of iterations (in addition, in this case, the uniformity of the field poses the regularization-based solution in good operating conditions). It can be observed that Gaussian prefiltering improves the quality of results and lowers the estimation errors. This is due to the fact that the test sequence has the same velocity values for each pixel in the image. It should be noted that the zeroth-order OFC-based solution presents an error in the angle comparable with that obtained at the 99th iteration with the Horn and Schunck solution. This confirms that the zeroth-order OFC-based solution produces optical flow that is qualitatively correct with respect to the velocity field. For the solutions of Tretiak and Pastor and of Haralick and Lee, very high estimation errors are provided in the absence of filtering, whereas lower errors are present in the other cases, i.e., demonstrating a strong sensitivity to noise. In addition, in this case, by using a postfiltering, there exists an improvement of estimation quality only for the algorithms of Haralick and Lee and that of Tretiak and Pastor (which is reported in the second part of the Table II. These algorithms present an additional improvement by using both prefiltering and postfiltering, but it can be noted that the highest improvement is registered by applying the postfiltering.

Occlusions: The synthetic sequence shown in Fig. 6, where two objects with a superimposed plaid pattern move in different directions, was chosen to test the behavior of the solutions in the presence of discontinuities due to occlusions. The estimation results are shown in Fig. 7. For the new EOFC- and OFC-based solutions, the presence of some optical flow field irregularities on the object boundaries can be observed, even though object profiles are still maintained. The first-order EOFC-based solution provides a better estimation with respect to the other multiconstraint solutions. Approaches by Haralick and Lee and Tretiak and Pastor produce large estimation errors at the occlusion profiles. The approach by Horn and Schunck produces less satisfactory results due to the undesirable effect of optical flow field propagation on the occluded objects.

C. Expansions and Contractions

As was pointed out in Section II, the difference between the OFC and the EOFC equations consists of the divergence of the velocity field. This term is very useful in evaluating the time-to-collision [7], [6] as well as for 3-D motion estimation and 3-D object structure reconstruction [1], [45]–[47].

Effects of divergence motion were tested using a sequence (see Fig. 8) that includes frames obtained by moving the camera toward the scene along the Z axis. Results obtained

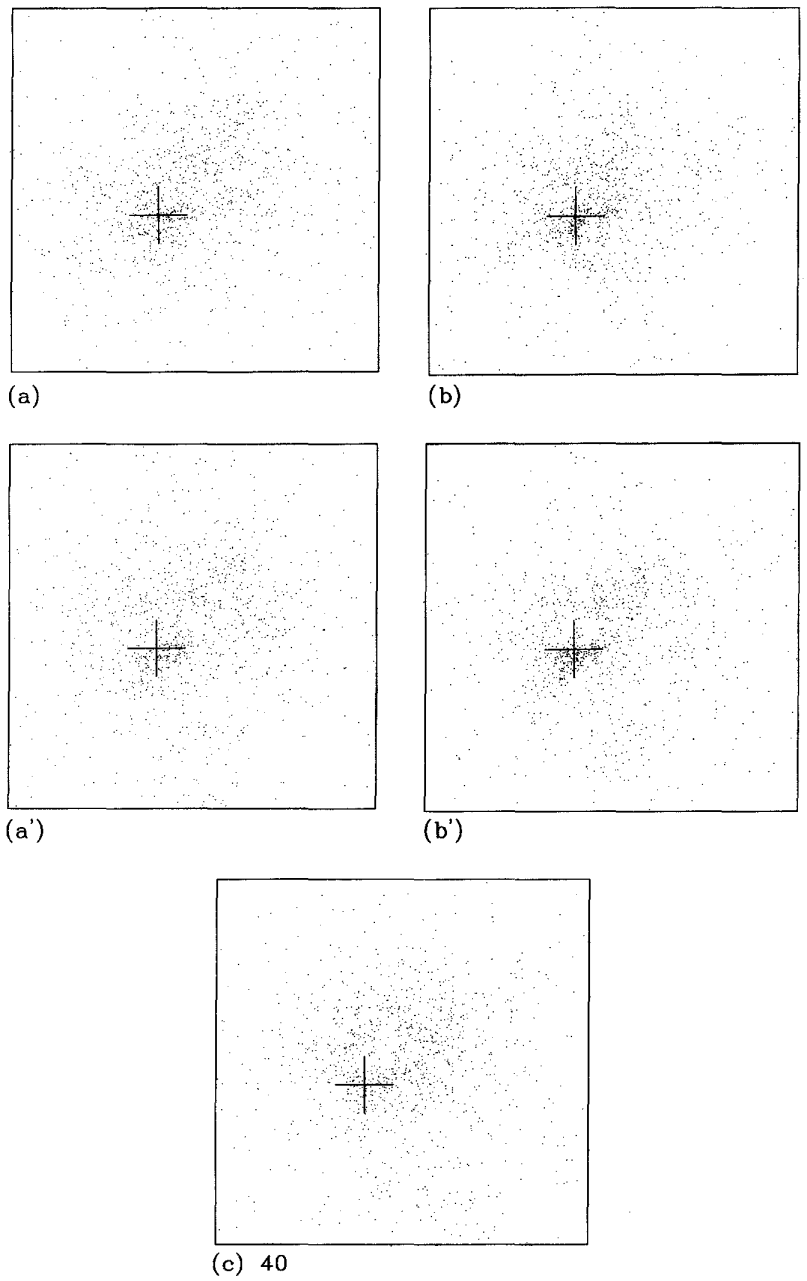

Fig. 10. Distribution of points $\mathbf{p}_{\mathrm{FOE}}$ for the sequence in Fig. 8 derived from the optical flow field presented in Fig. 9: (a) Zeroth-order EOFC-based solution; (b) first-order EOFC-based solution; (a′) zeroth-order OFC-based solution; (b′) first-order OFC-based solution; (c) Horn and Schunck OFC-based solution (40th iteration); (d) Haralick and Lee multiconstraint OFC-based solution; (e) Tretiak and Pastor OFC-based direct solution. The cross identifies the actual FOE.

with $N = 3$ are presented in Fig. 9. It should be noted that both OFC-based solutions provide the best estimation quality. Among the others, the Haralick and Lee solution also appears to produce good results. Comparing the multipoint techniques, the OFC-based solutions give better results in the central part of the image, whereas the EOFC-based techniques give better results in the outer parts of the image. An explanation of this behavior with respect to divergence motion is reported in [24].

The error analysis has been carried out by taking into account the distribution of the focus of expansion (FOE). The FOE is defined as the intersection point between the image plane and the axis of the instantaneous object-observer relative translation

$$\mathbf{p}_{\mathrm{FOE}} = \left(l\frac{W_1/Z}{W_3/Z}, l\frac{W_2/Z}{W_3/Z}, l \right)^t. \tag{16}$$

Rotational and translational components of 3-D motion can be distinguished when determining the focus of expansion, and hence, the motion of the observer (ego-motion) can be estimated [38], [48].

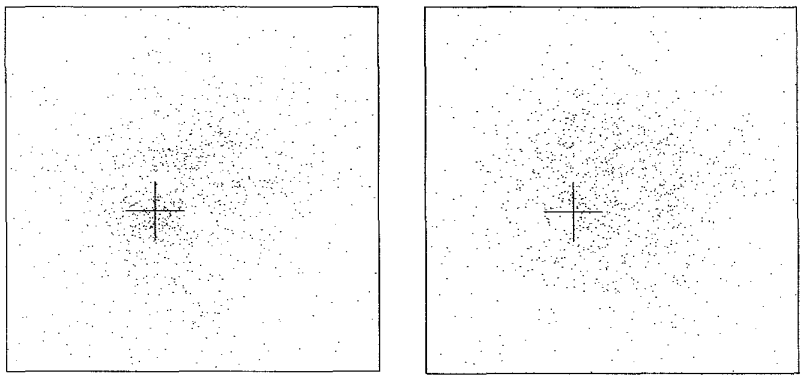

(d) (e)

Fig. 10. (Continued).

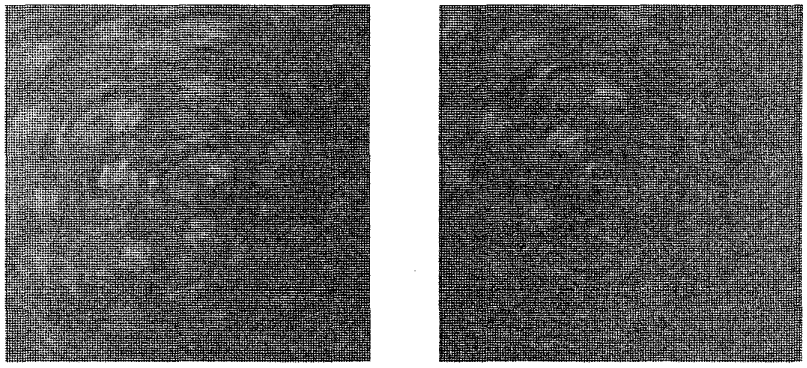

1 9

Fig. 11. Sequence of images with a regular pattern rotating around the Z-axis (first and ninth frame, 128×128 image resolution).

Fig. 10 shows the distribution of $\mathbf{p}_{\mathrm{FOE}}$ estimations. It can be observed that all the new solutions provide a more accurate estimation of the FOE. This can be recognized by observing a denser distribution of $\mathbf{p}_{\mathrm{FOE}}$ estimations in the proximity of the exact FOE (which is represented by a cross). The estimations of the FOE in Fig. 10 are evaluated by using (16), where the 3-D motion components are obtained as the least-square solution of an overdetermined linear system of (1) and (2) in six unknowns $(W_1/Z, W_2/Z, W_3/Z, \Omega_1, \Omega_2, \Omega_3)$ in a 5×5 grid of velocity field values.

D. Rotations

Rotations have been analyzed by using two test sequences with rotations around the Z axis and the X and Y axes, respectively.

Rotation Around the Z Axis: In the sequence of Fig. 11, a dense pattern placed on a planar patch parallel to the image plane moves in rotational motion around the Z axis. The rotational velocity is so high that large displacements in the points far from the center of rotation are produced. According to this, the motion (i.e., pixel displacements) can be measured only in the proximity of the rotation center. A radius of 10 pixels was assumed to identify the valid region.

The optical flow fields obtained for the analyzed solutions are presented in Fig. 12. Among the new solutions, results obtained (in the valid region) with EOFC are similar to those of OFC. This is in agreement with the conclusions drawn in [24]. The Tretiak and Pastor solution in Fig. 12(e) presents less satisfactory results with respect to the other methods due to its sensitivity to noise.

The averages of percentage errors of the absolute value of the angular velocity component $\Omega_3(\mathrm{Err}_{|\Omega_3|})$ estimated in the valid region are presented in Table III for the algorithms considered. The component Ω_3 was estimated according to

$$|\Omega_3| = \frac{\|\mathbf{V}\|}{\|\mathbf{p}\|}$$

which was obtained from (1) and (2), where $W_1 = 0, W_2 = 0, W_3 = 0, \Omega_1 = 0, \Omega_2 = 0$ were imposed. By observing Table III, it can be seen that a better estimation has been obtained with the zeroth-order OFC- and EOFC-based solutions, whereas the solution of Horn and Schunck tends to smooth the flow field, giving less satisfactory estimations when the number of iterations is high.

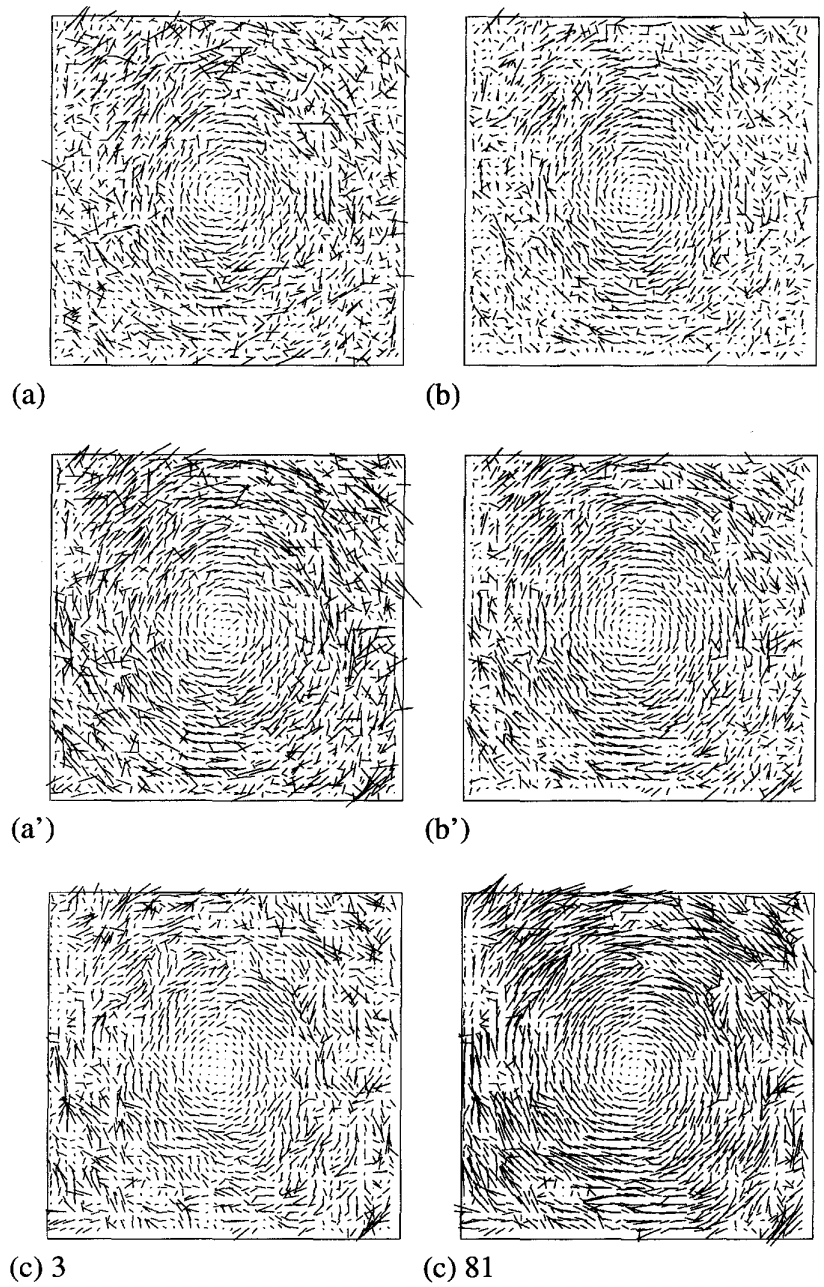

Fig. 12. Optical flow estimation referred of the fifth frame of the sequence in Fig. 11 obtained with (a) zeroth-order EOFC-based solution, $N = 3$; (b) first-order EOFC-based solution, $N = 3$; (a′) zeroth-order EOFC-based solution, $N = 3$; (b′) first-order EOFC-based solution, $N = 3$; (c) Horn and Schunck OFC-based solution (iterations: 3, 81), $\alpha = 0.6$; (d) Haralick and Lee multiconstraint OFC-based solution, 3×3 post-filtering; (e) Tretiak and Pastor OFC-based direct solution, 3 ×3 post-filtering.

Rotation Around the X and Y Axes To test the behavior of the algorithms in the presence of rotation around the X and Y axes, a sequence where a cylindrical body is moving under rotation around a transversal axis has been chosen. This axis of rotation is placed in a plane parallel to the image plane and rotated 45° with respect to the X axis (see Fig. 13). The values of Ω_1 and Ω_2 were estimated by considering (1) and (2) with $W_1 = 0, W_2 = 0, W_3 = 0, \Omega_3 = 0$. A system of two equations in two unknowns (the rotational components are Ω_1, Ω_2) is obtained, which is solved at any point where the velocity field can be estimated.

Results and estimations errors are shown in Table IV. It should be noted that estimations are affected by very large errors with respect to the other cases of motion. This is due to the fact that in these motion conditions, the optical flow field estimated by using the OFC is only an approximation of the velocity field [24]. A clockwise rotation is estimated in all approaches. In addition, in this case, the new zeroth-order

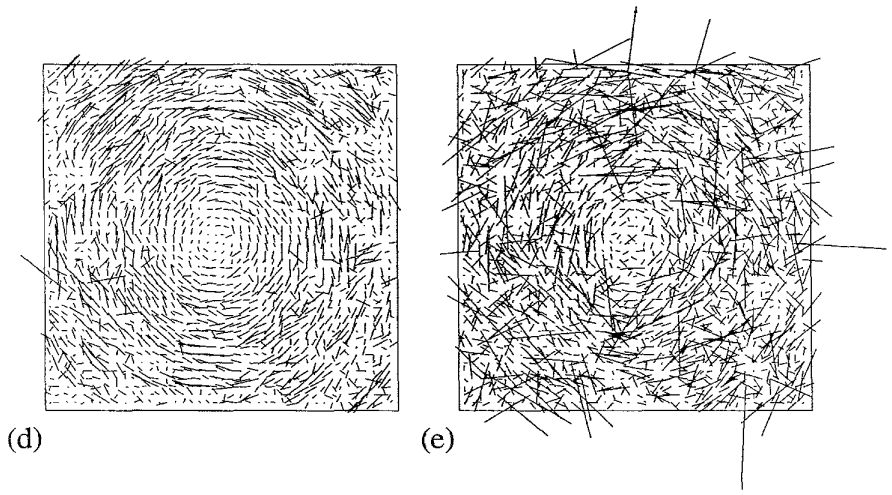

Fig. 12. (Continued).

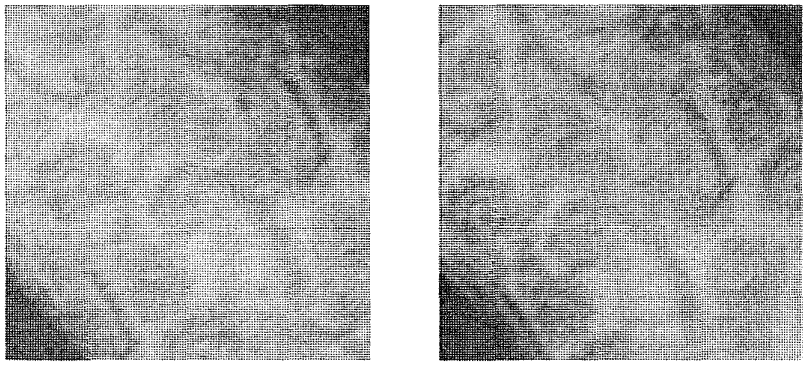

Fig. 13. Sequence of images with a pattern rotating around the X and Y axes (first and ninth frame, 128×128 image resolution).

EOFC- and OFC-based solutions provide better results with respect to the other solutions. Using the EOFC, lower error values are introduced according to [24]. The Horn and Schunck solution provides underestimations in the early iterations and leads to overestimations as the number of iterations grows. This is due to the propagation of the optical flow estimations.

E. Complexity

The explicit and asymptotical complexities for the compared solutions are reported in Table V. The following symbols are used for the parameters of interest:

- $M \times M$ size of the image,
- $N \times N$ size of the neighborhood,
- G distance between consecutive optical flow vectors expressed in pixels in both directions x, y,
- Q number of constraint equations for each pixel,
- F dimension of neighborhood in the case of a final optical flow field averaging,
- n number of unknowns,
- $O()$ asymptotical complexity,
- Sc scale factor of $O()$,
- I_t number of iterations (which is present only for the Horn and Schunck solution).

TABLE IV
ROTATIONAL VELOCITY COMPONENTS AROUND THE X AND Y AXES AND ESTIMATION ERRORS ($||\Omega|| = 1.482^\circ$ PER FRAME)

algorithm	Ω_1	Ω_2	$\|\|\Omega\|\|$	$Err_{\|\|\Omega\|\|}$
Zero-order EOFC-based	0.916	-1.029	1.377	7.00
First-order EOFC-based	0.798	-0.958	1.247	15.84
Zero-order OFC-based	0.992	-1.115	1.493	7.73
First-order OFC-based	0.921	-1.019	1.361	8.14
Horn & Schunck, 24th Iteration	0.809	-1.056	1.330	10.21
Horn & Schunck, 42th Iteration	1.125	-1.463	1.846	24.56
Horn & Schunck, 99th Iteration	1.127	-1.465	1.848	24.74
Haralick & Lee	0.900	-0.978	1.329	10.27
Tretiak & Pastor	0.532	-0.891	1.038	29.95

In Table V, if $N = G = F$, the asymptotical complexity is equal to M^2 for all the solutions, except for the solution of Horn and Schunck, where M^2 is multiplied by the number of the iterations I_t. If the distance among the estimation points is equal to 1 (i.e., $G = 1$), the solution of Horn and Schunck does not require a final averaging step, and its complexity is

TABLE V
COMPLEXITY AND PERFORMANCE COMPARISON. TIME IS THE ELAPSED CPU TIME EXPRESSED IN SECONDS OBTAINED ON AN 80386/80387 MACHINE AT 20 MHZ., WITH $N = G = F = 3, M = 128$

algorithm	Explicit Complexity	Q	n	Sc.	O()	Time
Zero-order EOFC	$M^2\left(Q + \frac{N^2}{G^2}Qn^2 + \frac{n^3}{G^2}\right)$	1	3	9	$\frac{M^2N^2}{G^2}$	30 ± 1
First-order EOFC	$M^2\left(Q + \frac{N^2}{G^2}Qn^2 + \frac{n^3}{G^2}\right)$	3	6	81	$\frac{M^2N^2}{G^2}$	340 ± 10
Zero-order OFC	$M^2\left(Q + \frac{N^2}{G^2}Qn^2 + \frac{n^3}{G^2}\right)$	1	2	5	$\frac{M^2N^2}{G^2}$	18 ± 1
First-order OFC	$M^2\left(Q + \frac{N^2}{G^2}Qn^2 + \frac{n^3}{G^2}\right)$	3	2	15	$\frac{M^2N^2}{G^2}$	117 ± 1
Horn & Schunck	$M^2\left(Q + I_t n^3\right)$	1	2	8	$M^2 I_t$	$I_t(14 \pm 1)$
Haralick & Lee	$M^2\left(Q + Qn^2 + n^3 + n\frac{F^2}{G^2}\right)$	4	2	2	$M^2\left(14 + \frac{F^2}{G^2}\right)$	146 ± 10
Tretiak & Pastor	$M^2\left(Q + n^3 + n\frac{F^2}{G^2}\right)$	2	2	2	$M^2\left(5 + \frac{F^2}{G^2}\right)$	75 ± 2

$I_t M^2$, whereas for the other solutions, this is equal to M^2N^2. Since most techniques have the same asymptotical complexity, for the sake of comparison, the table contains also a column that reports a scale factor Sc.

The last column of Table V shows the CPU time elapsed as obtained with $N = 3, G = 3, F = 3$, and $M = 128$, as measured on an 80 386/80 387 INTEL (20 MHz).

If the estimation quality is considered, it can be noted that results approximately similar to those obtained with the new techniques with $G = N = 3$ are obtained (although with a certain resolution loss in the moving object boundaries) with the same G and the following:

i) $F = 3$ for the Haralick and Lee solution
ii) $F > 7$ for Tretiak and Pastor solution
iii) $I_t > 40$ for the solution of Horn and Schunck.

In this case, zeroth-order OFC- and EOFC-based techniques present the lowest complexity with respect to the other techniques.

V. CONCLUSION

In this paper, two new techniques for the estimation of optical flow have been proposed. Both techniques are based on an approximation (zero- and first-order, respectively) of the partial differential equations modeling the changes in the image brightness and belong to the class of multiconstraint/multipoint approaches. These two techniques have been used with two distinct constraints. On the one hand, the classical optical flow constraint equation (OFC) has been employed. On the other hand, a constraint equation including the divergence of the optical flow field, referred to as extended optical flow constraint (EOFC) has been adopted. Results achieved in these four cases have been compared with selected solutions available in the literature for all the cases of 3-D motion.

As was shown, the proposed techniques produce solutions that are better ranked with respect to the other selected solutions in almost all motions analyzed. In the presence of discontinuities due to occlusions or object boundaries, a high insensitivity has been verified for the new techniques, whereas the other approaches have different undesirable effects such as estimation spreading (Horn and Schunck) or estimation errors (Haralick and Lee and Tretiak and Pastor).

Differences in the behavior of the analyzed solutions have been observed in the case of discontinuities due to noise. The analysis using synthetic image sequences showed better results with the Horn and Schunck technique, mainly due to the fact that a uniform plaid pattern was used in the test sequence. On the other hand, using an outdoor image sequence, the four multipoint solutions still appear to be better ranked. Among the new techniques, first-order solutions achieve qualitatively better results (mainly due to the higher number of constraint equations used per pixel) with respect to zeroth-order solutions that are more precize in estimating the velocity field but a little bit more sensitive to discontinuities.

No appreciable differences among the various techniques have been found in the presence of translational motion parallel to the image plane. On the other hand, expansion and contraction motions were better detected with the new techniques than with the others. In these cases, similar results are also achieved with the Haralick and Lee approach, whereas a spreading effect was observed with the Horn and Schunck solution. Results have been confirmed with error analysis. Zeroth-order solutions provide more satisfactory estimations for rotations around the Z axis. Several problems are encountered in this case with the other approaches, such as spreading (Horn and Schunck) and irregularities in the solutions (Tretiak and Pastor). Zeroth-order solutions are also definitely better ranked in the case of rotations around the X and Y axes.

Several differences have been observed between the solutions using EOFC and those using OFC. First-order solutions appear to be more robust in the presence of discontinuities. For expansion and contraction motions, OFC-based solutions provide better estimations in the region close to the image center, whereas EOFC-based solutions give better results in the outer parts of the image. No appreciable differences were observed in the other cases.

Finally, both zeroth-order solutions proposed in this paper are ranked higher as far as the computational complexity is concerned.

ACKNOWLEDGMENT

The authors wish to thank L. Reyna (IBM Yorktown Heights) for his valuable suggestions and help concerning the use of PDE's.

REFERENCES

[1] K. Prazdny, "On the information in optical flows," *Comput. Vision, Graphics, Image Processing*, vol. 23, pp. 239–259, 1983.

[2] G. Adiv, "Inherent ambiguities in recovering 3-d motion and structure from a noisy field," *IEEE Trans. Patt. Anal. Machine Intell.*, vol. 11, pp. 477–489, May 1989.

[3] P. J. Burt *et al.*, "Object tracking with a moving camera," in *Proc. IEEE Workshop Visual Motion*, IEEE Computer Society, Irvine, CA, USA, Mar. 20–22, 1989, pp. 2–12.

[4] T. J. Broida and R. Chellappa, "Experiments and uniqueness results on object structure and kinematics from a sequence of monocular images," in *Proc. IEEE Workshop Visual Motion*, IEEE Computer Society, Irvine, CA, USA, Mar. 20–22, 1989, pp. 21–30.

[5] A. Borri, G. Bucci, and P. Nesi, "A robust tracking of 3-D motion," in *Proc. Euro. Conf. Comput. Vision, ECCV'94*, Stockholm, Sweden, May 2–6, 1994, pp. 181–188.

[6] R. C. Nelson and J. Y. Aloimonos, "Obstacle avoidance using field divergence," *IEEE Trans. Patt. Anal. Machine Intell.*, vol. 11, pp. 1102–1106, Oct. 1989.

[7] M. Subbarao, "Bounds on time-to-collision and rotation component from first-order derivatives of image flow," *Comput. Vision, Graphics, Image Processing*, vol. 50, pp. 329–341, 1990.

[8] L. S. Davis, Z. Wu, and H. Sun, "Contour-based motion estimation," *Comput. Vision, Graphics, Image Processing*, vol. 23, pp. 313–326, 1983.

[9] J. H. Duncan and T. Chou, "Temporal edges: The detection of motion and the computation of optical flow," in *Proc. 2nd IEEE Int. Conf. Computer Vision ICCV '88*, Tampa, FL, USA, 1988.

[10] J. K. Aggarwal and N. Nandhakumar, "On the computation of motion from sequences of images—A review," *Proc. IEEE*, vol. 6, pp. 917–935, Aug. 1988.

[11] T. S. Huang and A. N. Netravali, "3-D motion estimation," in *Machine Vision for Three-Dimensional Scenes*. New York: Academic, 1990, pp. 195–219.

[12] E. H. Adelson and J. R. Bergen, "Spatiotemporal energy models for the perception of motion," *J. Opt. Soc. Amer. A*, vol. 2, pp. 284–299, Feb. 1985.

[13] D. Heeger, "Model for the extraction of image flow," *J. Opt. Soc. Amer. A*, vol. 4, pp. 1455–1471, Aug. 1987.

[14] L. Jacobson and H. Wechsler, "Derivation of optical flow using a spatiotemporal-frequency approach," *Comput. Vision, Graphics, Image Processing*, vol. 38, pp. 29–65, 1987.

[15] G. L. Fennema and W. B. Thompson, "Velocity determination in scene containing several moving objects," *Comput. Graphics, Image Processing*, vol. 9, pp. 301–315, 1979.

[16] B. K. P. Horn and B. G. Schunck, "Determining optical flow," *Artificial Intell.*, vol. 17, pp. 185–203, 1981.

[17] H.-H. Nagel, "Displacement vectors derived from second-order intensity variations in image sequences," *Comput. Vision, Graphics, Image Processing*, vol. 21, pp. 85–117, 1983.

[18] R. M. Haralick and J. S. Lee, "The facet approach to optical flow," in *Proc. Image Understanding Workshop*, L. S. Baumann, Ed. Arlington, VA: Science Applications, 1983.

[19] O. Tretiak and L. Pastor, "Velocity estimation from image sequences with second order differential operators," in *Proc. 7th IEEE Int. Conf. Patt. Recogn.*, 1984, pp. 16–19.

[20] A. Verri, F. Girosi, and V. Torre, "Differential techniques for optical flow," *J. Opt. Soc. Amer. A*, vol. 7, pp. 912–922, May 1990.

[21] B. G. Schunck, "Image flow: Fundamentals and future research," in *Proc. IEEE Conf. Comput. Vision Patt. Recogn., CVPR '85*, San Francisco, CA, USA, June 19–23, 1985, pp. 560–571.

[22] A. Verri and T. Poggio, "Motion field and optical flow: Qualitative properties," *IEEE Trans. Patt. Anal. Machine Intell.*, vol. 11, pp. 490–498, May 1989.

[23] H.-H. Nagel, "On a constraint equation for the estimation of displacement rates in image sequences," *IEEE Trans. Patt. Anal. Machine Intell.*, vol. 11, pp. 13–30, Jan. 1989.

[24] A. DelBimbo, P. Nesi, and J. L. C. Sanz, "Analysis of optical flow constraints," *IEEE Trans. Image Processing*, vol. 4, pp. 460–469, Apr. 1995.

[25] J. Hadamard, *Lectures on the Cauchy Problem in Linear Partial Differential Equations*. New Haven, CT: Yale University Press, 1923.

[26] H.-H. Nagel and W. Enkelmann, "Toward the estimation of displacement vector fields by 'oriented smoothness' constraints," in *Proc. 7th IEEE Int. Conf. Patt. Recogn.*, Montreal, Canada, July 30–Aug. 2, 1984, pp. 6–8.

[27] ——, "An investigation of smoothness constraints for the estimation of displacement vector fields from image sequences," *IEEE Trans. Patt. Anal. Machine Intell.*, vol. PAMI-8, pp. 565–593, Sept. 1986.

[28] J. Konrad and E. Dubois, "Multigrid bayesian estimation of the image motion fields using stochastic relaxation," in *Proc. 2nd IEEE Int. Conf. Comput. Vision ICCV '88*, Tampa, FL, USA, 1988, pp. 354–362.

[29] P. Nesi, "Variational approach for optical flow estimation managing discontinuities," *Image Vision Comput.*, vol. 11, no. 7, pp. 419–439, 1993.

[30] E. C. Hildreth, "Computing the velocity field along contours," in *Motion: Representation and Perception*, N. I. Badler and J. K. Tsotsos, Eds. New York: Elsevier, 1986, pp. 121–127.

[31] R. J. Woodham, "Multiple light source optical flow," in *Proc. 3rd IEEE Int. Conf. Comput. Vision ICCV '90*, Osaka, Japan, Dec. 4–7, 1990, pp. 42–46.

[32] A. Mitiche, Y. F. Wang, and J. K. Aggarwal, "Experiments in computing optical flow with the gradient-based multiconstraint method," *Patt. Recogn.*, vol. 20, no. 2, pp. 173–179, 1987.

[33] P. Nesi, A. DelBimbo, and D. Ben-Tzvi, "A robust algorithm for optical flow estimation," *Comput. Vision, Graphics, Image Processing: Image Understanding*, 1995.

[34] C. Cafforio and F. Rocca, "Tracking moving objects in television images," *Signal Processing*, vol. 1, pp. 133–140, 1979.

[35] M. Campani and A. Verri, "Computing optical flow from an overconstrained system of linear algebraic equations," in *Proc. 3rd IEEE Int. Conf. Comput. Vision ICCV '90*, Osaka, Japan, Dec. 4–7, 1990, pp. 22–26.

[36] P. Nesi, A. DelBimbo, and J. L. C. Sanz, "Multiconstraints-based optical flow estimation and segmentation," in *Proc. Int. Workshop Comput. Architecture Machine Perception*, Paris, Dec. 1991, pp. 419–426.

[37] B. G. Schunck, "The motion constraint equation for optical flow," in *Proc. 7th IEEE Int. Conf. Patt. Recogn.*, 1984, pp. 20–22.

[38] C. Longuet-Higgins and K. Prazdny, "The interpretation of a moving retinal image," *Proc. Roy. Soc. London B*, vol. 208, pp. 385–397, 1980.

[39] M. Born and E. Wolf, *Principle of Optics*. New York: Pergamon, 1959.

[40] B. K. P. Horn, *Robot Vision*, Cambridge, MA, London, New York, St. Louis, San Francisco: MIT Press, McGraw-Hill, 1986.

[41] J. A. Perrone, "In search of the elusive flow field," in *Proc. IEEE Workshop Visual Motion*, Irvine, CA, USA, IEEE Computer Society, Mar. 20–22, 1989, pp. 181–188.

[42] M. Yamamoto, "A general aperture problem for direct estimation of 3-D motion parameters," *IEEE Trans. Patt. Anal. Machine Intell.*, vol. 11, pp. 528–536, May 1989.

[43] A. Singh, *Optic Flow Computation: A Unified Perspective*. Los Alamitos, CA: IEEE Comput. Soc., 1991.

[44] P. Danielsson, P. Emanuelsson, K. Chen, P. Ingelhag, and C. Svensson, "Single-chip high-speed computation of optical flow," in *Proc. Int. Workshop Machine Vision Applications, MVA '90 IAPR*, Tokyo, Nov. 28–30, 1990, pp. 331–335.

[45] A. M. Waxman and S. Ullman, "Surface structure and three-dimensional motion from image flow kinematics," *Int. J. Robotics Res.*, vol. 4, no. 3, pp. 72–94, 1985.

[46] G. Adiv, "Determining three-dimensional motion and structure from optical flow generated by several moving objects," *IEEE Trans. Patt. Anal. Machine Intell.*, vol. PAMI-7, pp. 384–401, Apr. 1985.

[47] S. Ullman, "The optical flow of planar surfaces," *Spatial Vision*, vol. 1, no. 4, pp. 263–276, 1986.

[48] R. Jain, "Direct computation of the focus of expansion," *IEEE Trans. Patt. Anal. Machine Intell.*, vol. PAMI-5, pp. 58–64, Jan. 1983.

Alberto Del Bimbo (M'90) was born in Firenze, Italy, in 1952. He received the doctoral degree in electronics engineering from the Università di Firenze, Italy, in 1977.

He was with IBM ITALIA from 1978 to 1988. He is Full Professor of Computer Systems at the University of Florence, Italy. His research interests and activities are in the fields of image analysis, image databases, visual languages and virtual reality.

Dr. Del Bimbo is a member the International Association for Pattern Recognition (IAPR). He is on the board of the IAPR Technical Committee n. 8 (Industrial Applications) and the Vice-President of the IAPR Italian Chapter. He presently serves as Associate Editor of *Pattern Recognition* and of the *Journal of Visual Languages and Computing*.

Paolo Nesi (M'92) was born in Florence, Italy, in 1959. He received the doctoral degree in electronic engineering from the University of Florence, Italy. In 1992, he received the Ph.D. degree in electronic and informatics engineering from the University of Padoa, Italy.

In 1991, he was a visitor at the IBM Almaden Research Center, San Jose, CA. Since November 1991, he has been with the Department of Systems and Informatics at the University of Florence, Italy, as a Researcher and Assistant Professor of both Computer Science and Software Engineering. Since 1987, he has been invloved in different research topics including motion analysis, machine vision, physical models, parallel architectures, formal languages, real-time systems, and quality. He is an editorial board member of the *Journal of Real-Time Imaging* and the project manager of DIM45 ESPRIT III MEPI for the University of Florence. He has been a member of the program committe of international conferences and workshops and was General Chair of *Objective Quality 1995*, LNCS. He was the Editor of the *Journal of Real-Time Imaging* special issue on Real-Time Motion Analysis.

Dr. Nesi is a member of IAPR and AIIA.

Jorge L. C. Sanz (M'82–SM'86) was born in Buenos Aires, Argentina, in 1955. He received the Master degree in computer science in 1977 and in mathematics in 1978, both from the University of Buenos Aires. In 1981, he received the Ph.D. degree in applied mathematics, working on complexity of algorithms, from the same University.

His areas of broad professional interest are computer science and applied mathematics. Specifically, he is interested in multidimensional signal and image processing, image analysis, machine vision, parallel processing, numerical analysis, computer architectures, and other subjects. He was with the University of Buenos Aires as an instructor from 1978 to 1980. He was a Visiting Scientist at the Coordinated Science Laboratory, University of Illinois at Urbana-Champaign, USA, from 1981 to 1982 and was an Assistant Professor in 1983. He was with the Computer Science Department of the IBM Almaden Research Laboratory, San Jose, CA, USA, from 1984 to 1994. He was the Technical Manager of the Machine Vision Group from 1985 to 1986. Since 1985, he has also been an Adjunct Associate professor with the University of California at Davis, USA. He is presently Full Professor of Computer Science at the Coordinated Science Laboratory, University of Illinois at Urbana-Champaign. He is an Editor-in-Chief of *Machine Vision and Applications, An International Journal* (New York: Springer-Verlag). He is an author of the book *Random and Projection Transform-Based Computer Vision* (New York: Springer-Verlag, 1988). He is the Editor of the book *Advances in Machine Vision* (New York: Springer-Verlag). In 1986, he received the IEEE Acoustics, Speech, and Signal Processing Society's Paper Award.

Dr. Sanz is a member of the Multidimensional Signal Processing Committee of the IEEE Signal Processing Society. Since August 1987, he has been an Associate Editor of the IEEE TRANSACTIONS ON ACOUSTICS, SPEECH, AND SIGNAL PROCESSING. He was Editor of the IEEE TRANSACTIONS ON PATTERN ANALYSIS AND MACHINE INTELLIGENCE 1988 special issues on Industrial Machine Vision and Computer Vision Technology. He has been Chair and organizer of several Conferences and Workshops. He is an active member of ACM.